Demonstration of Entanglement-Enhanced Covert Sensing

Shuhong Hao,[1] Haowei Shi,[2] Christos N. Gagatsos,[2] Mayank Mishra,[2] Boulat Bash,[3,2] Ivan Djordjevic,[3,2] Saikat Guha,[2,3] Quntao Zhuang,[3,2] and Zheshen Zhang[1,3,2,*]

[1]*Department of Materials Science and Engineering, University of Arizona, Tucson, Arizona 85721, USA*
[2]*James C. Wyant College of Optical Sciences, University of Arizona, Tucson, Arizona 85721, USA*
[3]*Department of Electrical and Computer Engineering, University of Arizona, Tucson, Arizona 85721, USA*

(Received 10 December 2021; accepted 25 May 2022; published 27 June 2022)

The laws of quantum physics endow superior performance and security for information processing: quantum sensing harnesses nonclassical resources to enable measurement precision unmatched by classical sensing, whereas quantum cryptography aims to unconditionally protect the secrecy of the processed information. Here, we present the theory and experiment for entanglement-enhanced covert sensing, a paradigm that simultaneously offers high measurement precision and data integrity by concealing the probe signal in an ambient noise background so that the execution of the protocol is undetectable with a high probability. We show that entanglement offers a performance boost in estimating the imparted phase by a probed object, as compared to a classical protocol at the same covertness level. The implemented entanglement-enhanced covert sensing protocol operates close to the fundamental quantum limit by virtue of its near-optimum entanglement source and quantum receiver. Our work is expected to create ample opportunities for quantum information processing at unprecedented security and performance levels.

DOI: 10.1103/PhysRevLett.129.010501

Introduction.—Quantum information processing (QIP) hinges on nonclassical effects such as superposition and entanglement to enable new communication [1–4], sensing [5–11], and computing [12,13] capabilities beyond the reach of classical physics. Among these, quantum cryptography [14–16] has been envisaged to shift the landscape of information security and has migrated from proof-of-concept demonstrations in laboratory settings [14–20] to real-world intercontinental links relayed by a satellite [21–23]. Quantum cryptography protocols have now been embodied in a variety of realms, including blind quantum computing [24], decision making [25], and information gathering [26], to safeguard information from being acquired by an adversary.

Quantum covert protocols have recently emerged to offer a feature beyond the scope of these quantum cryptography protocols—the executions of the very protocols, with a high probability, are undetectable from the adversary's perspective [27–35], thereby ensuring the data integrity. The covertness of these protocols is fundamentally guaranteed by the indistinguishability between quantum states and hence can be quantified by the quantum measurement theory. In analogy to many quantum cryptography protocols [36–38], quantum covert protocols may be solely constructed upon classical transmitters and receivers [27,28,31,32,39–41], but quintessential quantum resources such as entanglement may offer additional performance gains. Indeed, the benefit of entanglement in quantum covert protocols has been recently analyzed [3,32,42], but an experimental realization for entanglement-enhanced covert systems remains elusive.

In this Letter, we propose and experimentally implement an *entanglement-enhanced* covert sensing protocol and benchmark its performance against covert sensing based on classical resources [43] first presented in Refs. [39,41]. Both protocols are proven quantum optimum in their own classes, and our experiment demonstrates that an entanglement transmitter, in conjunction with a quantum receiver, enables a 46.5% reduction of the mean squared error (MSE) in estimating the phase imparted by an interrogated object, corresponding to a 87.6% signal-to-noise ratio improvement. Remarkably, the entanglement-enhanced covert sensing experiment operates at only 10% off the ultimate quantum limit for the MSE. This work would spark new QIP applications fueled by entanglement-enhanced security and performance.

Protocols.—Sketched in Fig. 1, the covert sensor comprises an entanglement transmitter and a quantum receiver, aimed at probing the phase shift imparted by an object situated in a lossy and noisy environment characterized by the overall transmissivity κ_E and the average per-mode background-noise photon number N_B. In covert sensing, the transmitter prepares M copies of entangled signal-idler mode pairs, represented as $\hat{\rho}_{SI}^{\otimes M}$, with on average N_S photons per mode. The idler modes are locally retained in a quantum memory with efficiency κ_I. The transmissivity for the signal modes within the entanglement transmitter is κ_T. The signal modes are exploited to interrogate a phase shift θ imparted by an object, yielding the global state

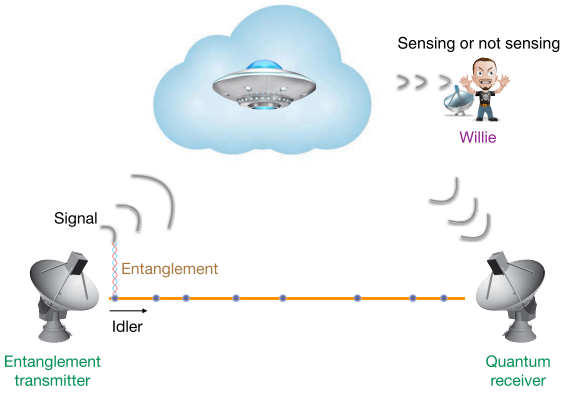

FIG. 1. Configuration for entanglement-enhanced covert sensing. Entanglement transmitter generates entangled signal and idler and sends the signal to probe an object. The quantum receiver performs a joint measurement on the signal returned from a lossy and noisy environment and the locally stored idler. Willie takes the optimal quantum measurement to detect the sensing attempt.

$\hat{\rho}'^{\otimes M}_{SI}(\theta)$. Accounting for the channel loss and environmental background noise, each signal mode at the quantum receiver carries on average N_B noise photons. The overall transmissivity between the entanglement source and the quantum receiver is defined as $\kappa \equiv \kappa_T \kappa_E$. The quantum receiver takes a joint measurement on the signal-idler mode pairs to generate an estimator for the phase: $\mathcal{M}_Q[\hat{\rho}'^{\otimes M}_{SI}(\theta)] \to \hat{\theta}_Q$. The estimation precision is quantified by the root-mean-square (rms) error $\delta\theta_Q = \sqrt{\langle(\theta - \hat{\theta}_Q)^2\rangle}$ subject to the quantum Cramér-Rao bound (QCRB):

$$\delta\theta_Q^2 \geq \frac{1}{M\mathcal{J}}, \tag{1}$$

where $\mathcal{J}$ is the quantum Fisher information for the sensing protocol under investigation (see Ref. [44]).

To detect the sensing attempt, the adversary, Willie, captures the probe photons lost in the noisy environment and endeavors to discriminate between two quantum states: $\hat{\rho}_0^{\otimes M}$ for the sole background noise and $\hat{\rho}_1^{\otimes M}$ for the same background noise augmented by a weak probe signal. The lower bound of Willie's detection error probability under such a quantum-state discrimination problem is given by

$$\mathbb{P}_e^{(w)} \geq \frac{1}{2}\left(1 - \frac{1}{2}\|\hat{\rho}_0^{\otimes M} - \hat{\rho}_1^{\otimes M}\|_1\right) \geq \frac{1}{2} - \epsilon, \tag{2}$$

where $\|\hat{\rho}_0^{\otimes M} - \hat{\rho}_1^{\otimes M}\|_1$ is the trace distance between $\hat{\rho}_0^{\otimes M}$ and $\hat{\rho}_1^{\otimes M}$, and ϵ is the covertness parameter, which can be arbitrarily set by choosing N_S and M. Within the range for the operational parameters of interest [44],

$$\epsilon \propto \frac{\sqrt{M}N_S}{N_B}. \tag{3}$$

The entanglement-enhanced covert sensing protocol is benchmarked against covert sensing based on classical states to demonstrate a quantum advantage. In the classical protocol, the sensor employs M copies of the probe state, $\hat{\rho}_S^{\otimes M}$ with the same energy as the entanglement-enhanced case, to interrogate the same phase object, resulting in $\hat{\rho}'^{\otimes M}_S(\theta)$ at the quantum receiver. A measurement $\mathcal{M}_C[\hat{\rho}'^{\otimes M}_S(\theta)]$ then produces a phase estimator $\hat{\theta}_C$ with the rms error $\delta\theta_C$. The marginal states $\hat{\rho}_0^{\otimes M}$ and $\hat{\rho}_1^{\otimes M}$ for Willie are set identical in the entanglement-enhanced and classical protocols so that their performance levels are evaluated under the same covertness parameter.

Experiment.—Our experimental setup is illustrated in Fig. 2(a), with a detailed description found in Ref. [44]. The transmitter consists of a periodically poled lithium niobate (PPLN) crystal to generate nondegenerate entangled signal and idler modes each occupying an optical bandwidth of W. The signal photons are exploited to probe a phase shift θ induced by a phase modulator (PM) while the idler photons are locally stored in a spool of low-loss optical fibers. Sensing is executed over T seconds consuming $M = WT$

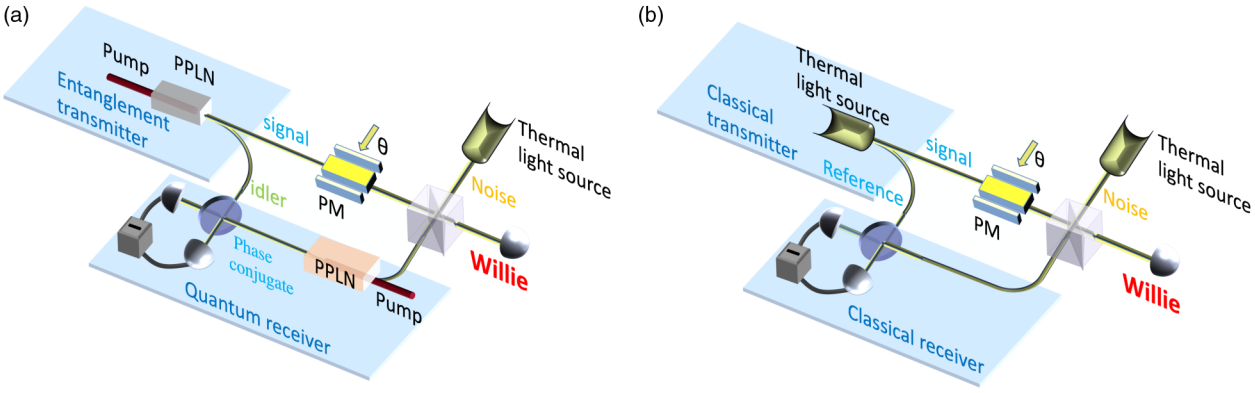

FIG. 2. Experimental setups for (a) entanglement-enhanced covert sensing and (b) covert sensing based on thermal light. Willie's apparatus to detect the sensing attempt is illustrated in Ref. [44]. PPLN, periodically poled lithium niobate; PM, phase modulator.

signal-idler mode pairs. The environmental noise is emulated by injecting thermal noise from an amplified spontaneous emission (ASE) source through a beam splitter. To infer the phase shift, a joint measurement is performed on the returned noisy signal and the retained idler modes in a phase-conjugate receiver (PCR) [52], which has been employed in entanglement-assisted communication to surpass the ultimate classical capacity [4]. In the PCR, the returned signal and the pump are combined at a second PPLN crystal to produce phase-conjugate modes via a low-gain difference-frequency generation process, through which the phase-sensitive cross-correlation between the signal and idler modes is carried over to the phase-insensitive cross-correlation between the phase-conjugate and idler modes, while only a small amount of noise in the signal modes is converted to the phase-conjugate modes. The wavelength of the phase-conjugate modes matches that of the idler modes, allowing them to interfere on a 50:50 beam splitter. The two output arms of the beam splitter are measured by a pair of photodetectors in a balanced setting to produce difference photocurrent, from which the phase estimator $\hat{\theta}_Q$ is acquired. The quantum advantage reaped by the PCR stems from the initial phase-sensitive cross-correlation between the entangled signal and idler modes. The residue phase-sensitive cross-correlation utilized by the PCR, albeit substantially weakened by the environment, remains much stronger than any classical probe and reference can deliver.

We also build a covert-sensing setup with classical resources as a performance benchmark [Fig. 2(b)]. In that experiment, the output of a thermal-light source is split into a signal arm and a reference arm. Compared to a coherent-light source, the thermal-light source features a large optical bandwidth proven advantageous for covert sensing [41]. The signal photons are modulated by the PM. At the homodyne receiver (HR), the returned signal photons mix with the reference on a 50:50 beam splitter followed by two photodetectors to take a balanced measurement that constructs the classical phase estimator $\hat{\theta}_C$.

To detect the sensing attempt, Willie takes a measurement in the noise background on a portion of the signal photons. Since Willie's marginal states $\hat{\rho}_0$ and $\hat{\rho}_1$ are both thermal, direct photon counting on a photodetector constitutes his optimal measurement for this quantum-state discrimination task to infer the presence of the probe. Willie's error probability in detecting the sensing attempt is tested by repeating a series of such measurements taken with or without the probe signal.

We first assess the performance of phase estimation in terms of the rms errors for both covert sensing protocols subject to the same covertness parameter ϵ, achieved by setting the brightness of the probes identical. An electro-optic modulator applies test phase shifts $\theta \in [0, \pi]$ on the probe in either sensing scenario. With appropriate scaling factors, the output of the PCR and the HR yield,

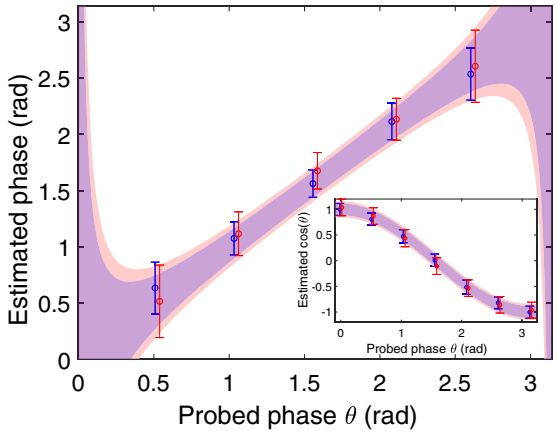

FIG. 3. Phase estimation in entanglement-enhanced covert sensing (blue) and classical covert sensing (red). Dots are experiment data, each obtained from averaging over 2000 consecutive measurements. Error bars represent rms errors. Shades represent the theoretical rms. Inset: estimation of $\cos(\theta)$. The probed phase values for classical (entanglement-enhanced) covert sensing are shifted on abscissa by 0.015 (−0.015) for readability. $N_S = 8 \times 10^{-4}$, $N_B = 160$, $T = 125$ μs, and $\kappa = 0.0165$.

respectively, unbiased cosine estimators $\cos(\hat{\theta}_Q)$ and $\cos(\hat{\theta}_C)$, as plotted in the inset of Fig. 3. The experimental data show good agreement with the theoretical model, demonstrating a quantum advantage for entanglement-enhanced covert sensing, manifested as a reduced experimental (error bars) and theoretical (shaded areas) estimation rms error. The experimentally measured cosine estimation rms error averaged over all test phases arrives at 0.1220 ± 0.0088 for entanglement-enhanced covert sensing, as compared to 0.1614 ± 0.0036 for classical covert sensing. The uncertainties in the rms errors account for the source-brightness fluctuation caused by the power instabilities of the pump laser ($< \pm 1\%$), the ASE source ($< \pm 1\%$), and the free-space to fiber coupling efficiency variation ($< \pm 3\%$), along with other optical, electrical, and mechanical instabilities. To derive the phase estimators, we take the inverse function on the cosine estimators to acquire $\hat{\theta}_Q = \arccos[\cos(\hat{\theta}_Q)]$ and $\hat{\theta}_C = \arccos[\cos(\hat{\theta}_C)]$. Figure 3 depicts the estimated phases versus the applied phases, showing that the rms error of the phase estimator for entanglement-enhanced covert sensing is reduced by an average of 24.0% from that of classical covert sensing.

We next study the performance of covert sensing under two environmental conditions at increasing background noise levels: the fixed covertness regime in which the probe power is adjusted to render the estimation MSE and Willie's detection error probability unchanged, and the fixed probe power regime in which the covertness is enhanced at the cost of an increased estimation MSE.

In light of Eq. (3), one needs to increase the probe power at higher background noise levels to maintain a constant

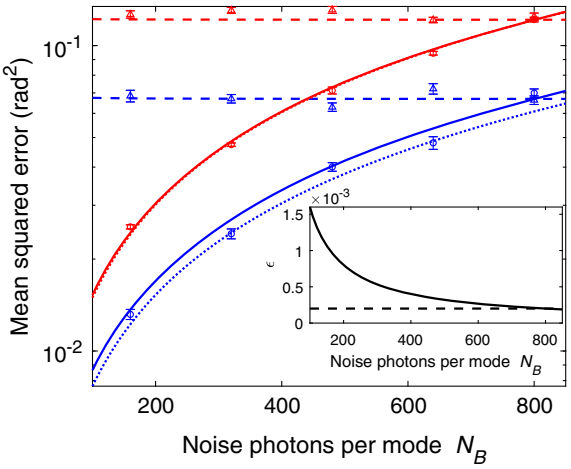

FIG. 4. MSE errors versus background-noise levels for entanglement-enhanced covert sensing (blue) and classical covert sensing (red). Experimental data (triangles) and theoretical model (dashed curves) in the fixed covertness regime; experimental data (circles) and theoretical model (solid curves) in the fixed probe power regime. Dotted lines: QCRBs in the fixed probe power regime. Inset: covertness parameter versus noise photons per mode for the fixed covertness (dashed line) and fixed probe power (solid line) regimes. $\theta = \pi/2$, $T = 125$ μs, $\kappa = 0.0165$. $N_S = 8 \times 10^{-4}$ for solid curves and QCRB; $N_S/N_B = 10^{-6}$ for dashed curves.

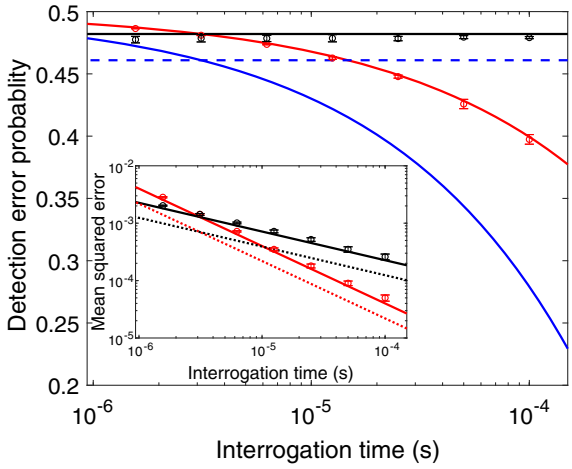

FIG. 5. Test of Willie's detection error probability when the square-root law is obeyed (black) or violated (red). Thermal-loss sensing channel emulated by a 50:50 beam splitter ($\kappa_E = 0.5$). $N_B = 1280$. $\kappa N_S\sqrt{M} = 200$ to obey the square-root law (black and blue dashed curve). $\kappa N_S/N_B = 6.25 \times 10^{-5}$ to violate the square-root law (red and blue curves). Dots: experimental data. Red and black curves: theory. Blue curves: lower bound for Willie's detection error probability. Inset: corresponding MSEs for classical (solid) and entanglement-enhanced (dotted) covert sensing around $\theta = \pi/2$, showing different scaling behaviors in obeying or violating the square-root law. MSE data for entanglement-enhanced covert sensing not taken due to limited photon flux at the source.

N_S/N_B in the fixed ϵ regime. Choosing $\epsilon = 2 \times 10^{-4}$ over a sensing channel with transmissivity $\kappa_E = 0.36$, the measured estimation MSEs (triangles) in Fig. 4 show an expected constant behavior and an excellent agreement with the theoretical model (dashed lines). The estimation MSEs for the entanglement-enhanced covert sensing (blue) situate below those for classical covert sensing (red), thereby demonstrating a quantum advantage. The estimation MSEs (circles) in the fixed probe power regime also closely match the theoretical model (solid lines). Notably, the measured estimation MSEs approach the QCRBs (dotted curves), showing that both the entanglement-enhanced and classical covert sensing protocols are operating near their quantum optima. The corresponding covertness parameters in the two regimes are plotted in the inset of Fig. 4.

Equation (3) dictates that the per-mode probe photon number N_S needs to scale as $1/\sqrt{M}$ to maintain a constant covertness parameter at a given background noise level, leading to a square-root scaling for the signal-to-noise ratio with respect to the number of employed signal-idler mode pairs, viz. $MN_S/N_B \propto \sqrt{M}$, which is a signature for covert communication and sensing protocols [27,28,31–35,39–41]. We experimentally test the square-root law and report the result in Fig. 5. Willie's detection error probabilities are measured at a range of M's by varying the interrogation time T. Following the square-root law of $N_S \propto 1/\sqrt{M}$, Willie's detection error probabilities stay at a constant at a cost of a reduced slope for the MSE versus T scaling, as illustrated by the experimental data (black dots) and the associated theoretical model (black curve) in Fig. 5. In contrast, fixing probe power irrespective of the interrogation time violates the square-root law, resulting in an undesired reduction of Willie's detection error probabilities, as evidenced in the experimental data (red dots) and theory (red curve). The scaling of MSEs in obeying or violating the square-root law is illustrated in the inset of Fig. 5, unveiling a trade-off between the measurement precision and covertness.

Discussion.—The PCR being optimum for entanglement-enhanced covert sensing but suboptimum for quantum illumination [52] unveils the fundamental disparity between two sensing regimes, parameter estimation and hypothesis testing. This situation is in analogy to phase estimation versus quantum-state discrimination based on coherent states: the HR is known to saturate the QCRB in estimating a phase shift imparted on a coherent state but fails to approach the ultimate Helstrom bound for discriminating two coherent states. Remarkably, the advantage of entanglement-enhanced covert communication protocols over their classical counterparts can scale as $1/\log(N_S)$ [3,32], which diverges as $N_S \to 0$. This quantum advantage is in sharp contrast to the constant quantum advantage enabled by quantum illumination [53–57]. Apart from being different from quantum illumination in the sensing

regimes, entanglement-enhanced covert sensing bears a security constraint—the signal power and interrogation time need to be carefully chosen subject to the channel and covertness parameters.

Similar to covert communication, covert sensing hides the probe light in the noisy environment; however, the two tasks differ in their aims and figures of merit. Specifically, covert communication is evaluated by the number of bits that can be covertly transmitted while covert sensing concerns about the precision of parameter estimation. Both covert communication and sensing, be they based on classical or quantum resources, assume that the strong noise background is uncontrollable by Willie. Such a passive scenario would be well justified in the microwave domain where the natural blackbody radiation noise is abundant in the background. The blackbody radiation, however, is negligible at optical wavelengths, so that achieving covertness in optical communication or sensing needs to rest upon other effective background noise such as the sunlight or the internet traffic. Our present proof-of-concept covert sensing experiments are carried out at optical wavelengths but can be adapted to the microwave domain by leveraging efficient microwave-photonic transducers [58].

Conclusions.—We have demonstrated entanglement-enhanced covert sensing approaching the fundamental quantum limit set by the QCRB. The verified entanglement-enabled quantum advantage would pave a new route for quantum-enhanced secure sensing, communication, and information processing.

This work is supported by Raytheon Technologies and in part by the Office of Naval Research (ONR) Grant No. N00014-19-1-2190 and National Science Foundation (NSF) Grants No. ECCS-1920742, No. CCF-1907918, No. CCF-2045530, and No. EEC-1941583. Q. Z. also acknowledges Defense Advanced Research Projects Agency (DARPA) under Young Faculty Award (YFA) Grant No. N660012014029. We thank Mark J. Meisner and Jaim Bucay for insightful discussions about the applications of the quantum technology.

*zsz@arizona.edu

[1] C. H. Bennett, P. W. Shor, J. A. Smolin, and A. V. Thapliyal, Entanglement-Assisted Classical Capacity of Noisy Quantum Channels, Phys. Rev. Lett. **83**, 3081 (1999).

[2] A. K. Ekert, Quantum Cryptography Based on Bell's Theorem, Phys. Rev. Lett. **67**, 661 (1991).

[3] H. Shi, Z. Zhang, and Q. Zhuang, Practical Route to Entanglement-Assisted Communication Over Noisy Bosonic Channels, Phys. Rev. Applied **13**, 034029 (2020).

[4] S. Hao, H. Shi, W. Li, J. H. Shapiro, Q. Zhuang, and Z. Zhang, Entanglement-Assisted Communication Surpassing the Ultimate Classical Capacity, Phys. Rev. Lett. **126**, 250501 (2021).

[5] V. Giovannetti, S. Lloyd, and L. Maccone, Quantum Metrology, Phys. Rev. Lett. **96**, 010401 (2006).

[6] V. Giovannetti, S. Lloyd, and L. Maccone, Advances in quantum metrology, Nat. Photonics **5**, 222 (2011).

[7] LIGO Scientific Collaboration, A gravitational wave observatory operating beyond the quantum shot-noise limit: Squeezed light in application, Nat. Phys. **7**, 962 (2011).

[8] J. Aasi, J. Abadie, B. Abbott, R. Abbott, T. Abbott, M. Abernathy, C. Adams, T. Adams, P. Addesso, R. Adhikari *et al.*, Enhanced sensitivity of the LIGO gravitational wave detector by using squeezed states of light, Nat. Photonics **7**, 613 (2013).

[9] M. Tse, H. Yu, N. Kijbunchoo, A. Fernandez-Galiana, P. Dupej, L. Barsotti, C. Blair, D. Brown, S. Dwyer, A. Effler *et al.*, Quantum-Enhanced Advanced LIGO Detectors in the Era of Gravitational-Wave Astronomy, Phys. Rev. Lett. **123**, 231107 (2019).

[10] Y. Xia, W. Li, W. Clark, D. Hart, Q. Zhuang, and Z. Zhang, Demonstration of a Reconfigurable Entangled Radio-Frequency Photonic Sensor Network, Phys. Rev. Lett. **124**, 150502 (2020).

[11] S. Pirandola, B. R. Bardhan, T. Gehring, C. Weedbrook, and S. Lloyd, Advances in photonic quantum sensing, Nat. Photonics **12**, 724 (2018).

[12] P. W. Shor, Polynomial-time algorithms for prime factorization and discrete logarithms on a quantum computer, SIAM Rev. **41**, 303 (1999).

[13] J. Biamonte, P. Wittek, N. Pancotti, P. Rebentrost, N. Wiebe, and S. Lloyd, Quantum machine learning, Nature (London) **549**, 195 (2017).

[14] S. Pirandola, U. L. Andersen, L. Banchi, M. Berta, D. Bunandar, R. Colbeck, D. Englund, T. Gehring, C. Lupo, C. Ottaviani *et al.*, Advances in quantum cryptography, Adv. Opt. Photonics **12**, 1012 (2020).

[15] F. Xu, X. Ma, Q. Zhang, H.-K. Lo, and J.-W. Pan, Secure quantum key distribution with realistic devices, Rev. Mod. Phys. **92**, 025002 (2020).

[16] I. Djordjevic, *Physical-Layer Security and Quantum Key Distribution* (Springer, Cham, Switzerland, 2019).

[17] J. Lodewyck, M. Bloch, R. García-Patrón, S. Fossier, E. Karpov, E. Diamanti, T. Debuisschert, N. J. Cerf, R. Tualle-Brouri, S. W. McLaughlin, and P. Grangier, Quantum key distribution over 25 km with an all-fiber continuous-variable system, Phys. Rev. A **76**, 042305 (2007).

[18] B. Korzh, C. C. W. Lim, R. Houlmann, N. Gisin, M. J. Li, D. Nolan, B. Sanguinetti, R. Thew, and H. Zbinden, Provably secure and practical quantum key distribution over 307 km of optical fibre, Nat. Photonics **9**, 163 (2015).

[19] Z. Zhang, Q. Zhuang, F. N. C. Wong, and J. H. Shapiro, Floodlight quantum key distribution: Demonstrating a framework for high-rate secure communication, Phys. Rev. A **95**, 012332 (2017).

[20] Z. Zhang, C. Chen, Q. Zhuang, F. N. Wong, and J. H. Shapiro, Experimental quantum key distribution at 1.3 gigabit-per-second secret-key rate over a 10 dB loss channel, Quantum Sci. Technol. **3**, 025007 (2018).

[21] S.-K. Liao, W.-Q. Cai, W.-Y. Liu, L. Zhang, Y. Li, J.-G. Ren, J. Yin, Q. Shen, Y. Cao, Z.-P. Li *et al.*,

Satellite-to-ground quantum key distribution, Nature (London) **549**, 43 (2017).
[22] S.-K. Liao, W.-Q. Cai, J. Handsteiner, B. Liu, J. Yin, L. Zhang, D. Rauch, M. Fink, J.-G. Ren, W.-Y. Liu *et al.*, Satellite-Relayed Intercontinental Quantum Network, Phys. Rev. Lett. **120**, 030501 (2018).
[23] J. Yin, Y. Cao, Y.-H. Li, J.-G. Ren, S.-K. Liao, L. Zhang, W.-Q. Cai, W.-Y. Liu, B. Li, H. Dai *et al.*, Satellite-to-Ground Entanglement-Based Quantum Key Distribution, Phys. Rev. Lett. **119**, 200501 (2017).
[24] S. Barz, E. Kashefi, A. Broadbent, J. F. Fitzsimons, A. Zeilinger, and P. Walther, Demonstration of blind quantum computing, Science **335**, 303 (2012).
[25] M. Ben-Or and A. Hassidim, Fast quantum byzantine agreement, in *Proceedings of the ACM Symposium on Theory of Computing (STOC)* (ACM, Baltimore, 2005), pp. 481–485.
[26] M. Ganz, Quantum leader election, Quantum Inf. Process. **16**, 73 (2017).
[27] B. A. Bash, A. H. Gheorghe, M. Patel, J. L. Habif, D. Goeckel, D. Towsley, and S. Guha, Quantum-secure covert communication on bosonic channels, Nat. Commun. **6**, 8626 (2015).
[28] A. Sheikholeslami, B. A. Bash, D. Towsley, D. Goeckel, and S. Guha, Covert communication over classical-quantum channels, in *Proceedings of the IEEE International Symposium on Information Theory (ISIT)* (IEEE, Barcelona, Spain, 2016).
[29] M. Tahmasbi and M. R. Bloch, Covert and secret key expansion over quantum channels under collective attacks, IEEE Trans. Inf. Theory **66**, 7113 (2020).
[30] M. Tahmasbi and M. R. Bloch, Toward undetectable quantum key distribution over bosonic channels, IEEE J. Sel. Areas Inf. Theory **1**, 585 (2020).
[31] M. S. Bullock, C. N. Gagatsos, S. Guha, and B. A. Bash, Fundamental limits of quantum-secure covert communication over bosonic channels, IEEE J. Sel. Areas Commun. **38**, 471 (2020).
[32] C. N. Gagatsos, M. S. Bullock, and B. A. Bash, Covert capacity of bosonic channels, IEEE J. Sel. Areas Inf. Theory **1**, 555 (2020).
[33] B. A. Bash, D. Goeckel, and D. Towsley, Square root law for communication with low probability of detection on AWGN channels, in *Proceedings of the IEEE International Symposium on Information Theory (ISIT)* (IEEE, Cambridge, MA, 2012).
[34] B. A. Bash, D. Goeckel, and D. Towsley, Limits of reliable communication with low probability of detection on AWGN channels, IEEE J. Sel. Areas Commun. **31**, 1921 (2013).
[35] B. A. Bash, D. Goeckel, D. Towsley, and S. Guha, Hiding information in noise: Fundamental limits of covert wireless communication, IEEE Commun. Mag. **53**, 26 (2015).
[36] F. Xu, J. M. Arrazola, K. Wei, W. Wang, P. Palacios-Avila, C. Feng, S. Sajeed, N. Lütkenhaus, and H.-K. Lo, Experimental quantum fingerprinting with weak coherent pulses, Nat. Commun. **6**, 1 (2015).
[37] H.-K. Lo, M. Curty, and B. Qi, Measurement-Device-Independent Quantum Key Distribution, Phys. Rev. Lett. **108**, 130503 (2012).
[38] H.-K. Lo, X. Ma, and K. Chen, Decoy State Quantum Key Distribution, Phys. Rev. Lett. **94**, 230504 (2005).
[39] B. A. Bash, C. N. Gagatsos, A. Datta, and S. Guha, Fundamental limits of quantum-secure covert optical sensing, in *Proceedings of the IEEE International Symposium on Information Theory (ISIT)* (IEEE, Aachen, Germany, 2017).
[40] D. Goeckel, B. A. Bash, A. Sheikholeslami, S. Guha, and D. Towsley, Covert active sensing of linear systems, in *Proceedings of the Asilomar Conference on Signals, Systems, and Computers* (IEEE, Pacific Grove, CA, 2017).
[41] C. N. Gagatsos, B. A. Bash, A. Datta, Z. Zhang, and S. Guha, Covert sensing using floodlight illumination, Phys. Rev. A **99**, 062321 (2019).
[42] M. Tahmasbi and M. R. Bloch, On covert quantum sensing and the benefits of entanglement, IEEE J. Sel. Areas Inf. Theory **2**, 352 (2021).
[43] In the remainder of the Letter we will use the term "classical covert sensing" for covert sensing based on classical resources, even though the security of such schemes is guaranteed by quantum mechanics.
[44] See Supplemental Material at http://link.aps.org/supplemental/10.1103/PhysRevLett.129.010501 for detailed description of the experimental setup, the calibration procedure, and the theoretical framework, which includes Refs. [45–51].
[45] R. S. Bennink, Optimal collinear Gaussian beams for spontaneous parametric down-conversion, Phys. Rev. A **81**, 053805 (2010).
[46] J. D. Franson, Nonlocal cancellation of dispersion, Phys. Rev. A **45**, 3126 (1992).
[47] J. H. Shapiro, Dispersion cancellation with phase-sensitive Gaussian-state light, Phys. Rev. A **81**, 023824 (2010).
[48] H. Scutaru, Fidelity for displaced squeezed thermal states and the oscillator semigroup, J. Phys. A **31**, 3659 (1998).
[49] P. Marian and T. A. Marian, Quantum Fisher information on two manifolds of two-mode Gaussian states, Phys. Rev. A **93**, 052330 (2016).
[50] C. N. Gagatsos, B. A. Bash, S. Guha, and A. Datta, Bounding the quantum limits of precision for phase estimation with loss and thermal noise, Phys. Rev. A **96**, 062306 (2017).
[51] S. Pirandola, R. Laurenza, C. Ottaviani, and L. Banchi, Fundamental limits of repeaterless quantum communications, Nat. Commun. **8**, 15043 (2017).
[52] S. Guha and B. I. Erkmen, Gaussian-state quantum-illumination receivers for target detection, Phys. Rev. A **80**, 052310 (2009).
[53] S.-H. Tan, B. I. Erkmen, V. Giovannetti, S. Guha, S. Lloyd, L. Maccone, S. Pirandola, and J. H. Shapiro, Quantum Illumination with Gaussian States, Phys. Rev. Lett. **101**, 253601 (2008).
[54] Z. Zhang, S. Mouradian, F. N. C. Wong, and J. H. Shapiro, Entanglement-Enhanced Sensing in a Lossy and Noisy Environment, Phys. Rev. Lett. **114**, 110506 (2015).
[55] J. H. Shapiro and S. Lloyd, Quantum illumination versus coherent-state target detection, New J. Phys. **11**, 063045 (2009).
[56] E. D. Lopaeva, I. Ruo Berchera, I. P. Degiovanni, S. Olivares, G. Brida, and M. Genovese, Experimental

Realization of Quantum Illumination, Phys. Rev. Lett. **110**, 153603 (2013).

[57] S. Barzanjeh, S. Guha, C. Weedbrook, D. Vitali, J. H. Shapiro, and S. Pirandola, Microwave Quantum Illumination, Phys. Rev. Lett. **114**, 080503 (2015).

[58] W. Jiang, C. J. Sarabalis, Y. D. Dahmani, R. N. Patel, F. M. Mayor, T. P. McKenna, R. Van Laer, and A. H. Safavi-Naeini, Efficient bidirectional piezo-optomechanical transduction between microwave and optical frequency, Nat. Commun. **11**, 1166 (2020).